

RESEARCH

Open Access



Femtomolar and locus-specific detection of N⁶-methyladenine in DNA by integrating double-hindered replication and nucleic acid-functionalized MB@Zr-MOF

Qingyuan Zheng^{1†}, Tong Wang^{1†}, Xinmin Li^{1,2}, Husun Qian¹, Xintong Bian¹, Xingrong Li¹, Huijie Bai¹, Shijia Ding¹ and Yurong Yan^{1*}

Abstract

In this study, a novel electrochemical biosensor was constructed for ultrasensitive and locus-specific detection of N⁶-Methyladenine (m⁶A) in DNA using double-hindered replication and nucleic acid-coated methylene blue (MB)@Zr-MOF. Based on the combination of m⁶A-impeded replication and Ag⁺-mediated mismatch replication, this mode could effectively stop the extension of the strand once DNA polymerase encountered m⁶A site, which specifically distinguish the m⁶A site from natural A site in DNA. Also, Zr-MOF with high porosity and negative surface potential features was carefully chose to load cationic MB, resulting a stable and robust MB@Zr-MOF electrochemical tag. As a result, the developed biosensor exhibited a wide linear range from 1 fM to 1 nM with detection limit down to 0.89 fM. Profiting from the high sensitivity and selectivity, the biosensing strategy revealed good applicability, which had been demonstrated by quantitating m⁶A DNA at specific site in biological matrix. Thus, the biosensor provides a promising platform for locus-specific m⁶A DNA analysis.

Keywords: N⁶-Methyladenine DNA, Double-hindered replication, MOF, Electrochemical biosensor

*Correspondence: yanyurong@cqmu.edu.cn

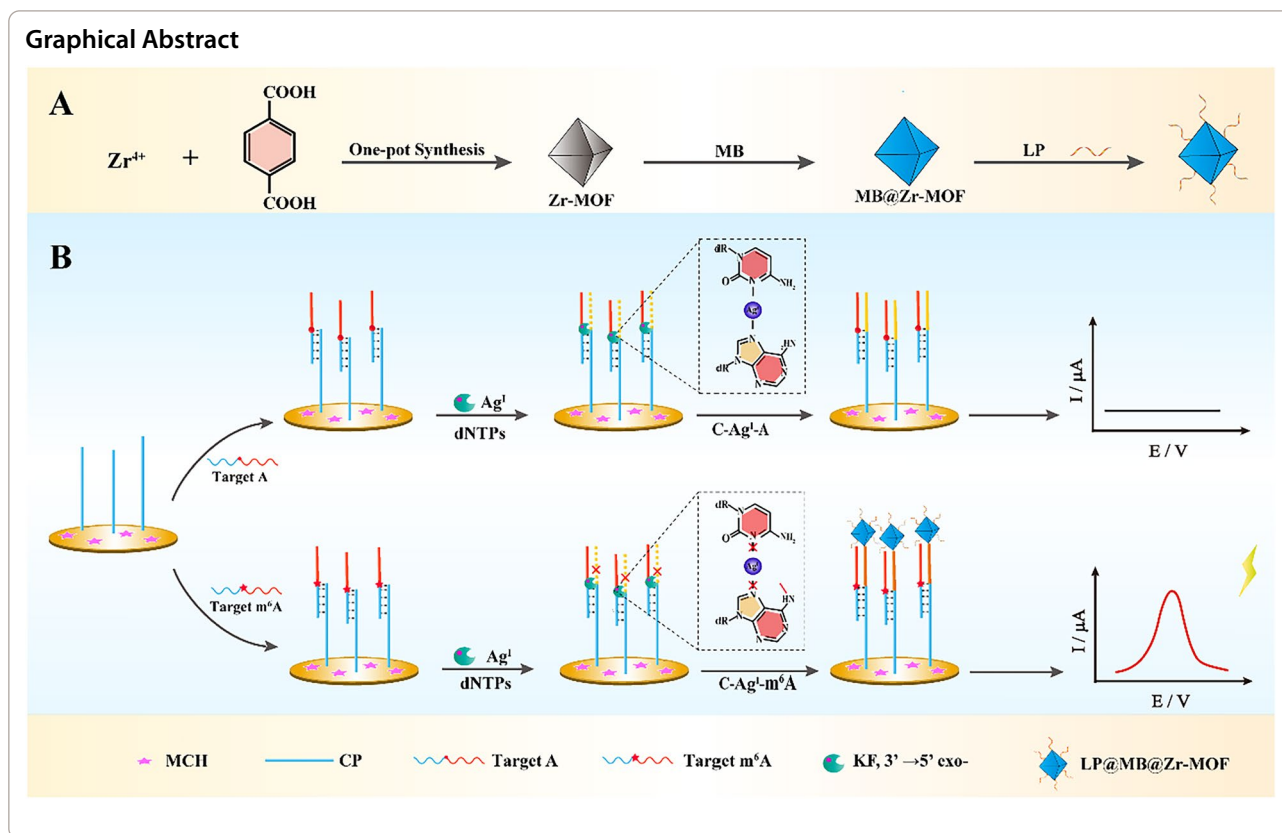
†Qingyuan Zheng and Tong Wang contributed equally to this work

¹ Key Laboratory of Clinical Laboratory Diagnostics (Ministry of Education), College of Laboratory Medicine, Chongqing Medical University, Chongqing 400016, China

Full list of author information is available at the end of the article



© The Author(s) 2021. **Open Access** This article is licensed under a Creative Commons Attribution 4.0 International License, which permits use, sharing, adaptation, distribution and reproduction in any medium or format, as long as you give appropriate credit to the original author(s) and the source, provide a link to the Creative Commons licence, and indicate if changes were made. The images or other third party material in this article are included in the article's Creative Commons licence, unless indicated otherwise in a credit line to the material. If material is not included in the article's Creative Commons licence and your intended use is not permitted by statutory regulation or exceeds the permitted use, you will need to obtain permission directly from the copyright holder. To view a copy of this licence, visit <http://creativecommons.org/licenses/by/4.0/>. The Creative Commons Public Domain Dedication waiver (<http://creativecommons.org/publicdomain/zero/1.0/>) applies to the data made available in this article, unless otherwise stated in a credit line to the data.



Introduction

Epigenetic modifications on nucleic acids could significantly regulate the long-term gene activity and expression [1–3]. In particular, N⁶-methyladenine (m⁶A) DNA, methylated at the N⁶ position of adenine in DNA, is one of the most important and prevalent heritable epigenetic modifications in bacteria and higher eukaryotic cells [4, 5]. In human cells, m⁶A/A ratio is ~0.056% in the blood genome DNA sample which means nM–pM levels of m⁶A DNA [6]. Recent studies have shown that m⁶A DNA is closely involved with DNA mismatch repair, chromosome replication, and cell-cycle regulation [7–9]. These characteristics enable m⁶A DNA to play an enigmatic role in physiological and pathological conditions, especially in the initiation and progression of cancers, such as ovarian cancer [10], liver cancer [11], and glioblastoma [12]. Thus, selective and sensitive quantitative analysis of m⁶A DNA is valuable for more understanding its biological functions and diagnosing cancers. However, it is still a challenge for the following reasons: the one is without any alteration in nucleotide sequence of m⁶A DNA, and the other is that m⁶A sites are not susceptible to chemical modifications [13, 14].

Previous methods for profiling of m⁶A DNA rely chiefly on next-generation sequencing [15–17] and modern

mass spectrometry [18]. Although these strategies provided powerful tools to gain the distribution information of m⁶A sites in genome, the requirement of expensive instruments, professional technical staff, and long analysis time has impeded their wide applications. Aim at these issues, several methods have been developed. For instance, Yeh et al. introduced m⁶A-specific silver nanocluster beacon relying on the diverse stabilities between A/m⁶A–G base pairs [19]. Owing to the small difference of stability generated from methyladenine only, the capacity of distinction between m⁶A and A of the method was limit. Additionally, Zhou' group reported primer extension-coupled electrophoresis separation strategy for the detection of m⁶A DNA utilizing the impediment of m⁶A to DNA synthesis [20]. Besides being unable to quantification and site-specific detection, this strategy was also difficult to distinguish m⁶A due to the fact that the optimal discernibility was gained in such a short extension time (1 min), which was attributed to the low selectivity of DNA polymerase towards m⁶A.

To improve the selectivity of m⁶A DNA detection, Ag^I-mediated formation of adenine (A) and cytosine (C) mismatch (A–Ag^I–C base pairs) by DNA polymerase has been applied. Specifically, DNA polymerase recognized Ag^I-mediated base pairs resulting in the incorporation

of a mismatched base into DNA primers through replication [21, 22]. In contrast, m⁶A site interfered the formation of the mismatch because of the steric hindrance caused by the bulky methyl group, which disturbed the recognition of DNA polymerase and stopped the replication [14]. Expanding the principle to ligase, Ag^I-mediated ligation and rolling circle amplification (RCA) [14] and Ag^I-assisted ligation coupled with hybridization chain reaction (HCR) [23] have been reported. Despite the significant difference between m⁶A and A in Ag^I-mediated ligation, the high nonspecific reactions of RCA and HCR need to be avoided [24, 25]. Also, the sensitivities of these strategies are insufficient owing to the ultralow m⁶A DNA amounts [4].

Metal–organic frameworks (MOFs) are a class of new organic/inorganic porous materials with high porosity, large surface area, and multiple functionalities [26–28]. Particularly, Zr-MOF with negative surface potential is an ideal carrier for adsorbing massive amounts of cationic tags such as methylene blue (MB), which is capable of enhancing its analysis sensibility [29–31]. On the other hand, thanks to the existence of Zr–P bond, Zr-MOF easily links to DNA strands [32]. Considering these unique characteristics, Zr-MOF is regarded as a promising material for constructing high-performance nucleic acid biosensors [33, 34]. Although MOF-based strategies have been developed for the detection of m⁶A DNA [35, 36], these methods still face the problems: low sensitivity, high cost owing to the usage of antibody, and the failure of sensing specific m⁶A sites. Thus, exploring MB@Zr-MOF as electrochemical tag provides a new way for developing m⁶A DNA detection method.

Inspired by these, we developed a novel electrochemical biosensor for ultrasensitive and site-specific detection of m⁶A DNA based on double-hindered replication and nucleic acid-functionalized MB@Zr-MOF. In this sensing system, once Klenow fragment (KF) DNA polymerase encountered m⁶A sites, the extension of capture probes (CP) hybridized with the part sequence of m⁶A DNA was terminated due to the double-hindered replication (the impediment of m⁶A to DNA synthesis and the failed recognition by DNA polymerase resulting from the instability of m⁶A–Ag^I–C mismatch in the absence of dTTPs). As a result, the remaining sequence of the m⁶A DNA was accessible. Then, linker probes (LP)-coated MB@Zr-MOF (LP@MB@Zr-MOF) bound to the free part of m⁶A DNA, thus gaining amplified electrochemical signal. Benefiting from the effective double-hindered replication and powerful signal amplification ability of MB@Zr-MOF, the developed biosensor provides a robust platform for femtomolar, single-base level and highly selective detection of m⁶A DNA without the involvement of any antibodies. Moreover, the biosensor holds the ability of site-specific

m⁶A DNA detection by simply adjust the sequence of capture probe.

Experimental section

Material and reagents

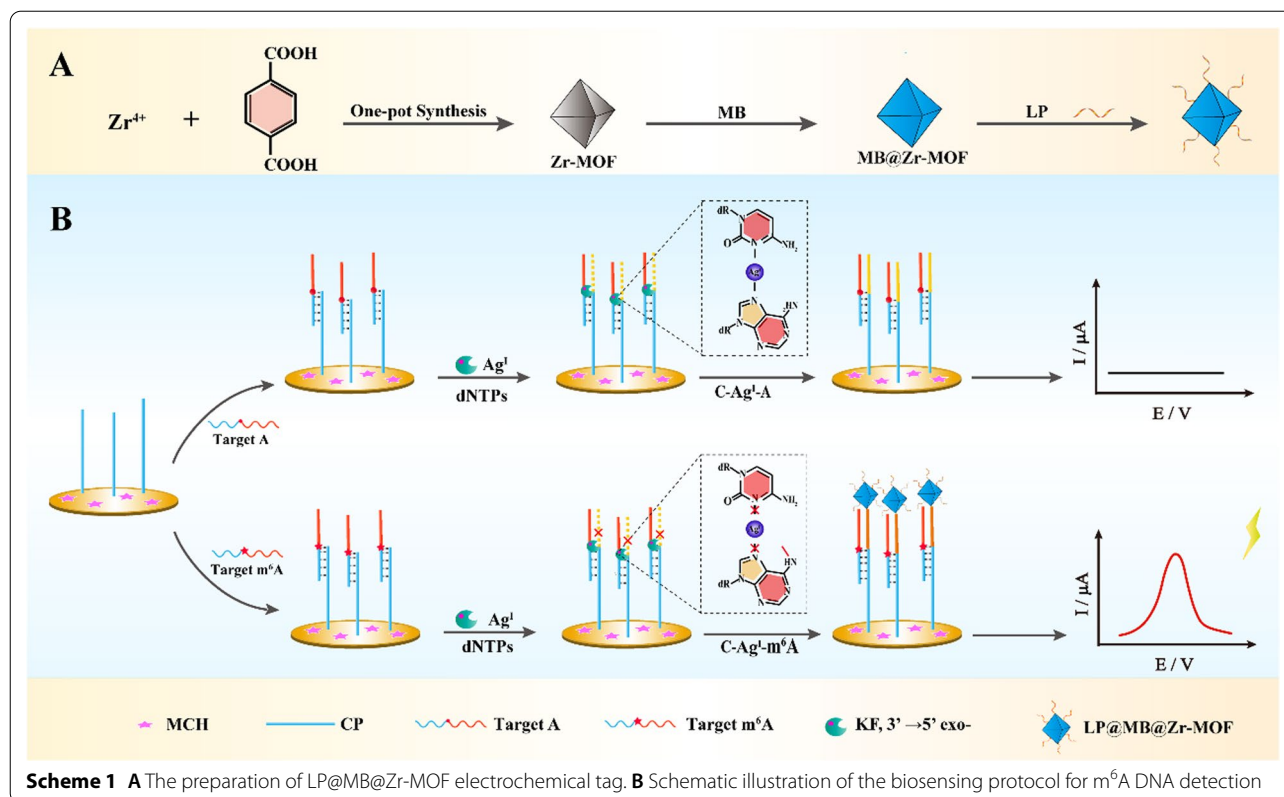
Klenow Fragment DNA polymerase (3'→5' exo⁻), 10 × Klenow buffer (500 mM Tris–HCl, 50 mM MgCl₂ and 10 mM DTT, pH 7.9), and 10 × CutSmart™ buffer (20 mM Tris–acetate, 500 mM potassium acetate, 10 mM magnesium acetate and 100 µg/mL BSA, pH 7.9) were obtained from New England Biolabs (Beijing, China). GoldView I, 20 bp DNA marker, and dATPs, dTTPs, dCTPs and dGTPs were purchased from SBS Genetech Co., Ltd., (Beijing, China), TaKaRa (Dalian, China), and Thermo Fisher Scientific Inc., (Waltham Mass, USA), respectively. Mercapto hexanol (MCH) and MB were provided by Sangon Biotech Inc. (Shanghai, China). All oligonucleotides (HPLC grade) used in this experiment were synthesized by Sangon Biotech Inc. (Shanghai, China) and TaKaRa (Dalian, China). The DNA sequences were illustrated in Additional file 1: Table S1. Milli-Q water (resistance of >18 MΩ cm) was used to prepare all solutions. All cell lines including normal human stem cells (NeHepLxHT) and liver cancer cells (HepG2) were obtained from American Type Culture Collection (ATCC, USA). The MethylFlash m⁶A DNA Methylation ELISA Kit (Colorimetric) was purchased from Epigentek (NY, USA).

Apparatus

Oligonucleotide concentrations were evaluated by a NanoDrop 1000 spectrophotometer (Thermo Scientific Inc., Wilmington, DE, USA). The electrophoretic gels were imaged by a ChemiDoc XRS system (Bio-Rad, Hercules, CA, USA). All electrochemical measurements were performed on a CHI660D Electrochemical Workstation (Shanghai Chenhua Instrument Co., Ltd., China) with a three-electrode electrochemical system including saturated calomel electrode as reference electrode, platinum electrode as counter electrode, and gold electrode (GE, 3 mm in diameter) as working electrode.

Synthesis of LP@MB@Zr-MOF

First, Uio-66 was synthesized according to the previous report with the slight modification [18]. A mixture of 75 mg zirconium tetrachloride (ZrCl₄), 782 mg benzoic acid, and 58 mg 2-aminoterephthalic acid (NH₂-BDC) was added into N, N'-dimethylformamide (DMF, 9 mL) in a 20 mL Teflon-lined stainless-steel reactor. After sonicated the mixture for about 10 min, the reactor was heated at 80 °C for 12 h, and held at 100 °C for another 24 h. After cooling down to room temperature, the resultant solid was collected by centrifugation for



5 min at 8000 rpm, then washed thoroughly with DMF and methanol. The gained Zr-MOF was placed under vacuum at 80 °C to remove the volatile methanol. Afterwards, MB@Zr-MOF was prepared by mixing 0.15 g Zr-MOF and 0.06 g MB in 50 mL methanol at 80 °C for 48 h. The solid was then filtered off, extensively washed with deionized water and methanol, and finally vacuum at 60 °C overnight. To synthesize LP@MB@Zr-MOF, the prepared MB@Zr-MOF was dissolved in 1 × PBS solution (pH 7.9) to form a 1 mg/mL of MB@Zr-MOF solution, then 1 μ M of LP was added in the solution and the mixture was stirred at 4 °C overnight. Subsequently, the baby blue product was collected by centrifugation (5 min, 8000 rpm) and then washed with 1 × PBS solution. Finally, the synthesized LP@MB@Zr-MOF was redissolved in 1 × PBS solution and stored at 4 °C for further use.

Fabrication of the proposed electrochemical biosensor

First, GE was polished with 0.05 μ M alumina powder for 5 min to a mirror, followed by sonication in ultrapure water, absolute ethanol and deionized water for 5 min, respectively. GE was then soaked in piranha solution for 10 min and rinsed thoroughly with deionized water for eliminating other impurity. 0.5 μ M CP was pretreated by Tris (2-carboxyethyl) phosphine (50 μ M) for 1 h to break

disulfide bond. Subsequently, 10 μ L of 0.5 μ M CP was dropped on the cleaned electrode followed by the incubation at 4 °C overnight. The prepared electrodes were washed with 1 × PBS solution (pH 7.4) and then covered with 10 μ L of 1 mM MCH for 0.5 h in room temperature to block the unbinding sites followed by rinsing with washing buffer.

For the m^6A DNA detection, 10 μ L of different concentrations of target was dropped onto the surface of the modified electrodes and incubated for 1 h at 37 °C to capture the target. Then, 10 μ L of reaction buffer including $AgNO_3$ (100 μ M), dNTP (1 μ M), KF (5 U), 10 mM Magnesium acetate, 8 mM DTT, 10 mM Tris-AcOH, and 100 mM AcOHNa, PH = 7.9) was added to the electrode surface and incubated at 37 °C for another 15 min for performing the Ag^+ -mediated DNA mismatch and replication. Subsequently, the electrode was incubated in 1 mg/mL of LP@MB@Zr-MOF solution at 37 °C for 1 h. Eventually, the electrodes were washed with 1 × PBS solution to remove unbound LP@MB@Zr-MOF for subsequent measurement.

Electrochemical measurements

Cyclic voltammetry (CV) and electrochemical impedance spectroscopy (EIS) measurements were conducted in 0.5 M KNO_3 solution containing 0.5 mM $[Fe(CN)_6]^{3/4-}$.

CV curves were recorded at scan rate of 10 mV s^{-1} and EIS spectra were collected with the frequency range from 0.1 MHz to 0.01 Hz. Meanwhile, the differential pulse voltammetry (DPV) measurements were performed in the working solution (0.1 M PBS, pH 7.4) with a pulse period of 0.5 s, a pulse width of 0.2 s, a pulse amplitude of 50 mV, and potential scan from -0.6 to 0.2 V .

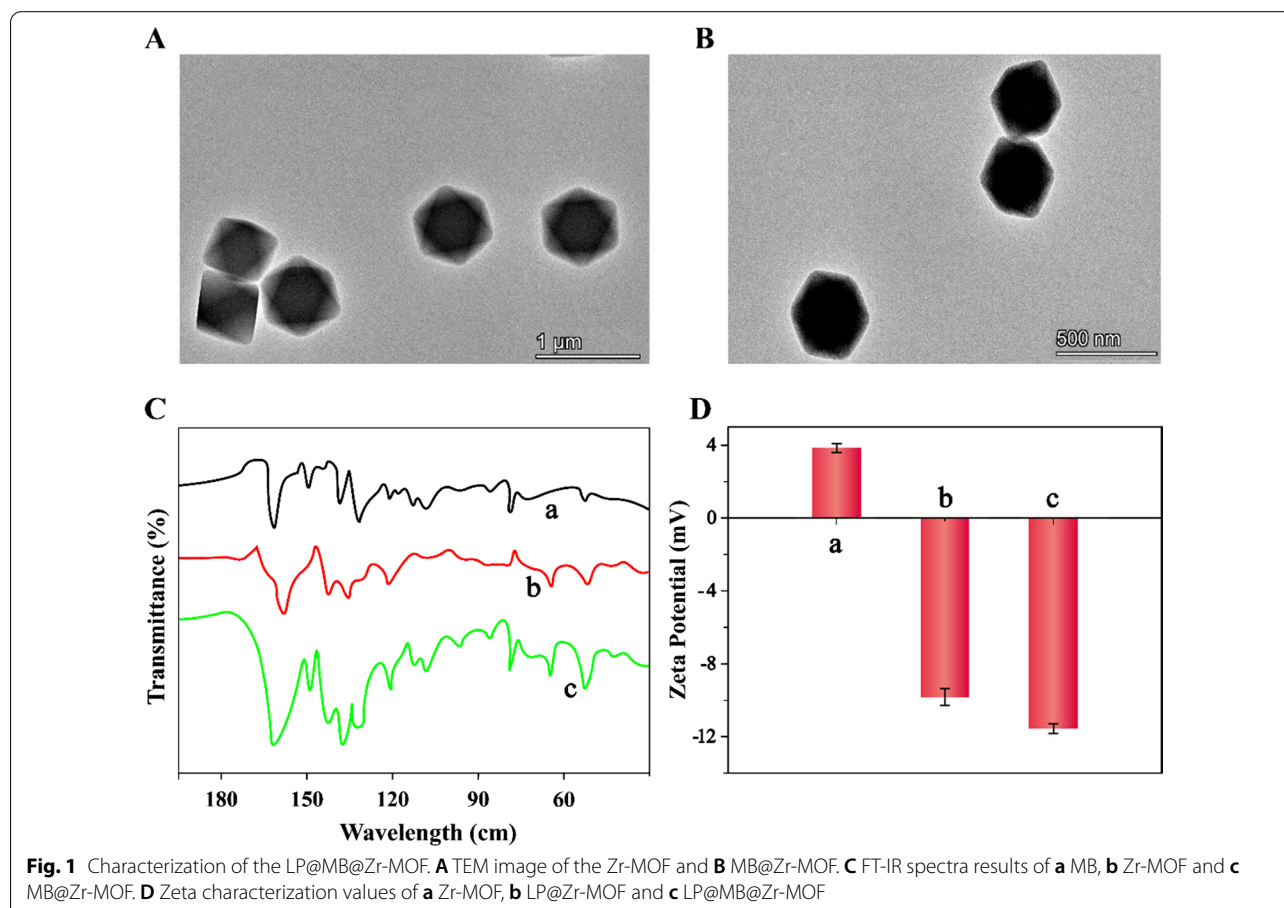
Gel electrophoresis

Twelve percent native polyacrylamide gel (PAGE) was prepared to verify the extension of primer by KF DNA polymerase and the effective distinguishment between target DNAs and target m^6A DNAs. Electrophoresis was carried in $1 \times$ TBE buffer (2 mM EDTA, 89 mM Tris-boric acid, pH 8.3) at a 100 V constant voltage for 45 min. Then, the gel was immersed in a freshly prepared stain solution (80 mL of $1 \times$ TBE buffer containing $4 \mu\text{L}$ of GoldView I) for 30 min. Afterwards, the gel was imaged using gel image system.

Cell culture and DNA extraction

The selected cells were cultured in DMEM containing 10% FBS and supplemented with $100 \mu\text{g/mL}$

streptomycin and 100 U/mL penicillin at $37 \text{ }^\circ\text{C}$ in a humidified incubator containing 5% CO_2 . The extraction steps of DNA from cells as follows: 1×10^6 HepG2 cells or NeHepLxHT cells was rinsed using cold PBS, and collected by centrifugation. After washing twice, 5 ml of DNA extraction buffer (10 mM Tris-HCl, 0.1 M EDTA, 0.5% SDS) were added. Then, $25 \mu\text{L}$ of proteinase K ($100 \mu\text{g/ml}$) was added and incubated for 3 h at $50 \text{ }^\circ\text{C}$. After that, a mixture of phenol, chloroform and isopentyl alcohol was used to extract the aqueous phase by centrifugation at 2500 r/min. Equal volume of LiCl (5 M) was added and incubated with ice bath for 10 min. The mixture was centrifuged at 2500 r/min for 10 min and the supernatant was transferred to a centrifuge tube which contained equal volume of isopropanol. After incubating for 10 min at room temperature, the product was collected through centrifugation at 2500 r/min for 10 min. Then, 0.1 times the volume of sodium acetate (3 M, pH = 5.2) and 2 times the volume of $-20 \text{ }^\circ\text{C}$ precooling anhydrous ethanol were added and the mixture was incubated at $-20 \text{ }^\circ\text{C}$ for 20 min. At last, the DNA extraction was separated by centrifugation at 12,000 r/min for 5 min and was redissolved in 1 ml TE buffer for further use.



Detection of m⁶A DNA in cells

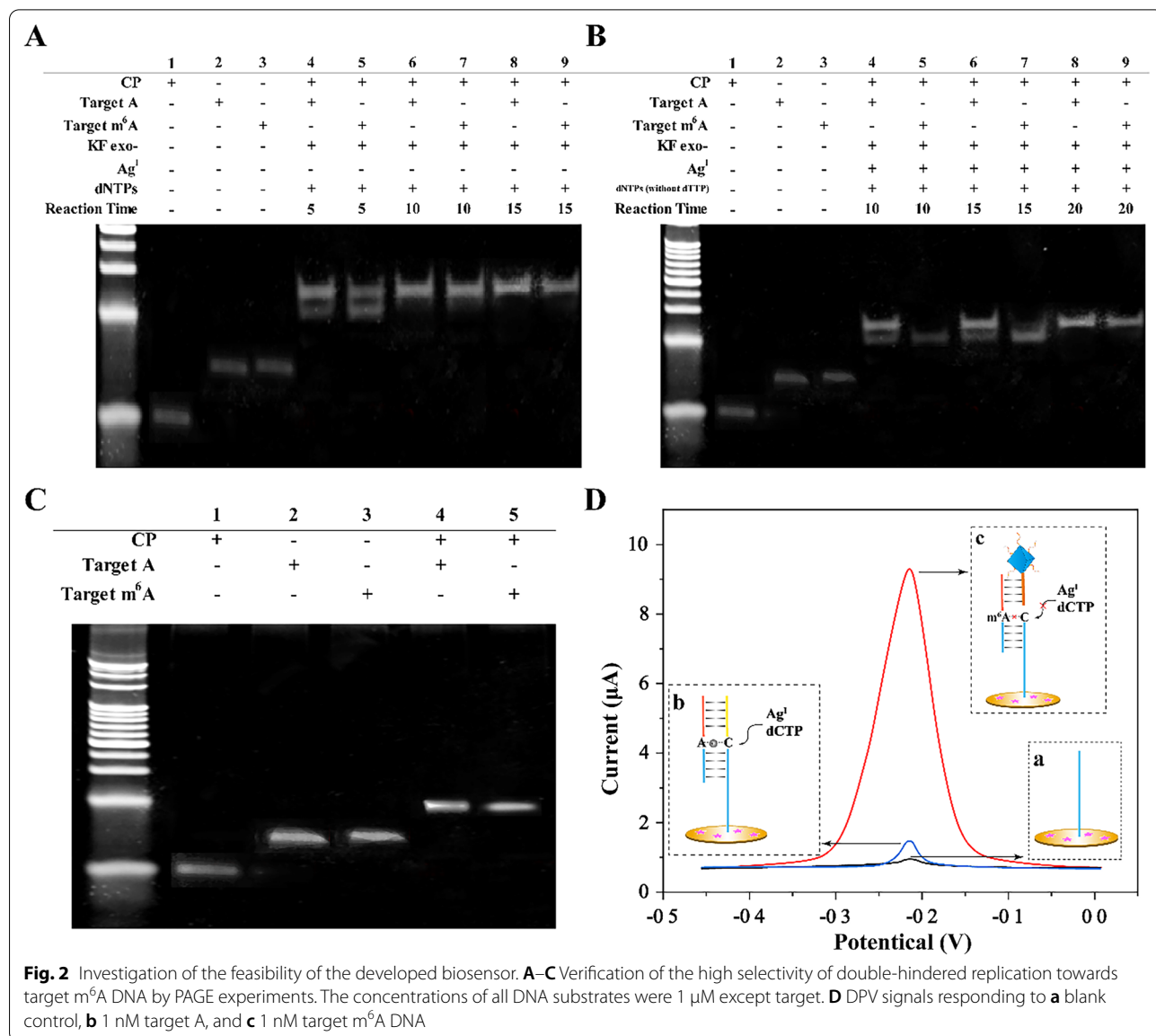
Different concentrations of cell's DNA extraction were tested using the proposed electrochemical biosensor and ELISA kit. The detection steps of the biosensor were according to the procedure proposed in "Fabrication of the proposed electrochemical biosensor" Section. ELISA analysis was conducted based on the product's principle and procedure.

Results and discussion

Operation principle of the electrochemical biosensor

The principle of the electrochemical biosensor for ultra-sensitive m⁶A DNA detection at a specific site by combining double-hindered replication with LP@MB@

Zr-MOF was illustrated in Scheme 1. In part A, Zr-MOF was synthesized by using a facile one-pot solvothermal reaction with NH₂-BDC as the ligand and Zr⁴⁺ as the metal nodes. Then, massive amounts of electroactive substrate MB were packed into Zr-MOF owing to its negative surface potential and high porosity, forming MB@Zr-MOF complex. Subsequently, the LP was linked with MB@Zr-MOF through Zr-P bonds, forming LP@MB@Zr-MOF electrochemical tag. The biosensing steps were shown in part B. Target DNA which was divided into two parts including CP and LP recognition domain by m⁶A site or A site was introduced and hybridized with CP. When there was an A site on the target DNA, KF DNA polymerase stabilized and replicated the mismatch A-C



with the existence of enough Ag^{I} and dNTPs (without dTTP). As a result, the LP recognition domain on target DNA would be blocked, leading to the failed binding of LP@MB@Uio-66 to electrode surface. However, when there was a m^6A site on target DNA, the incorporation of the mismatched C base into CP was stopped owing to the double-hindered replication caused by m^6A and the instability of $\text{m}^6\text{A}-\text{Ag}^{\text{I}}-\text{C}$. Therefore, LP recognition domain hybridized with the LP@MB@Zr-MOF, producing obvious electrochemical signal. Through the sensing strategy, target DNA with specific m^6A site was clearly distinguished from these with normal A site. Integration of the unique double-hindered replication and the excellent electrochemical activity of MB@Zr-MOF, the strategy realized ultrasensitive detection towards specific m^6A site in DNA.

Characterization of the LP@MB@Zr-MOF

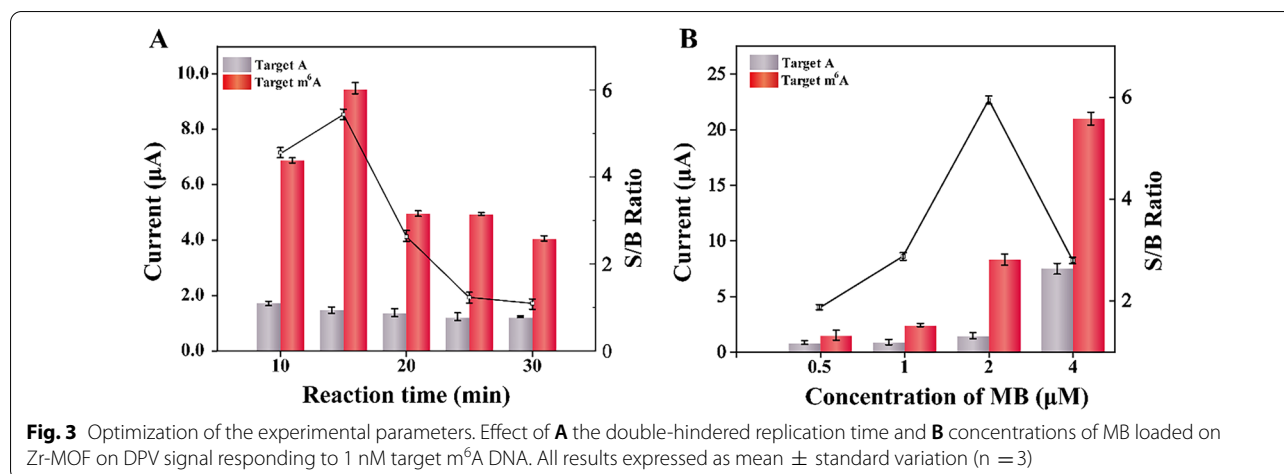
Transmission electron microscopy (TEM), FT-IR spectra, and Zeta potential experiment were performed to characterize the LP@MB@Zr-MOF. TEM images showed that the Zr-MOF (Fig. 1A) and MB@Zr-MOF crystals (Fig. 1B) had identical diameter, demonstrating that the little influence of MB on the morphologies of the prepared Zr-MOF. As depicted in Fig. 1C, FT-IR spectra exhibited the new peaks in the MB@Zr-MOF compared with that in Zr-MOF, indicating that MB was effectively encapsulated in Zr-MOF. As illustrate in Fig. 1D, the Zeta potential value of the Zr-MOF, LP@Zr-MOF, and LP@MB@Zr-MOF was about 3.8 mV, -10.32 mV, and -11.82 mV, respectively, demonstrating that Zr-MOF was modified by LP and MB. These results verified the successful synthesis of the LP@MB@Zr-MOF electrochemical indicator.

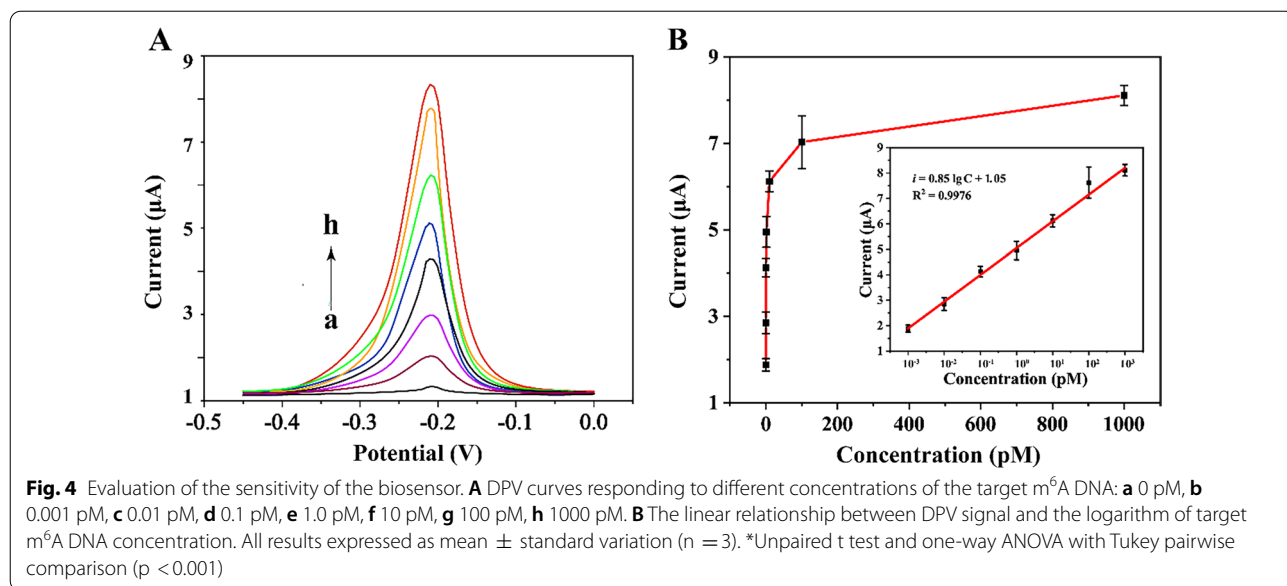
Characterization of the modification procedure on an electrode

CV and EIS were performed to characterize the step-wise electrode modification. Additional file 1: Fig. S1A gave the CV curves of various electrodes. It was obvious that a pair of redox peaks were observed at ~ 0.14 V and ~ 0.24 V on the GE (curve a). When the CP and MCH were immobilized on the electrode surface by turn, the peak current continued to decrease (curve b and c). Then, the binding of m^6A DNA to the modified electrode led to a decrease of peak current again (curve d). It might be explained that biomolecular modification blocked the electron-transfer between the electrolyte and electrode. However, when the LP@MB@Zr-MOF electrochemical indicator hybridized with the m^6A DNA, the peak current increased (curve e) owing to the electroactivity of MB@Zr-MOF. To evaluate the influence of biomolecules anchored on the electrodes, EIS was carried out (Additional file 1: Fig. S1B). The diameter of semicircle represented the electron-transfer resistance (Ret). It was found that the biomolecules on the electrode surface restricted the charge transfer when they were immobilized on the electrode surface. However, when the LP@MB@Zr-MOF was introduced, the Ret decreased (curve e). These results not only demonstrated the success of modification processes, but preliminarily confirmed the feasibility of the developed biosensor.

Feasibility of the sensing strategy for m^6A DNA detection

First, the double-hindered replication was investigated by PAGE experiment. As shown in Fig. 2A–C, lane 1, 2 and 3, in which each had a single band, represented CP, target A (wild-type DNA), and target m^6A DNA, respectively. See the results in Fig. 2C, the band location of the dsDNA-1 hybridized by CP and target A (lane 4) is

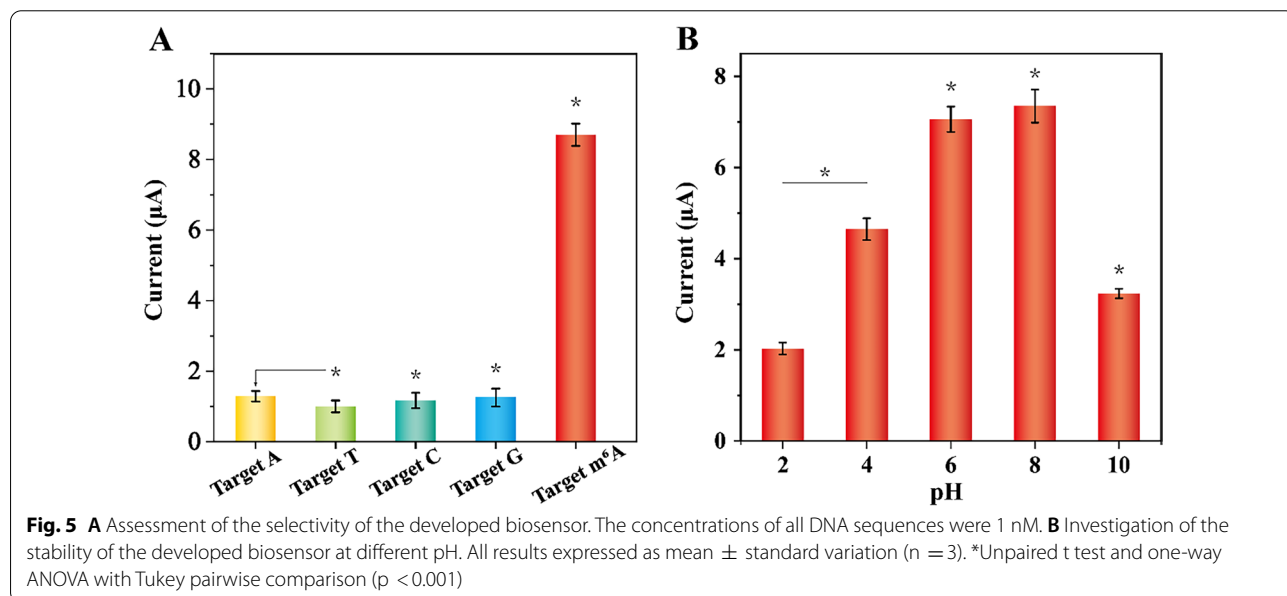




consistent with that of dsDNA-2 constructed by CP and target m⁶A DNA (lane 5), indicating that m⁶A site did not affect the hybridization of dsDNA. As seen in Fig. 2A, dsDNA, KF exo⁻, and dNTPs were mixed and incubated at 37 °C for 5 min (lane 4 and 5), 10 min (lane 6 and 7) and 15 (lane 8 and 9) min. However, both dsDNA-1 and dsDNA-2 were replicated in the first 5 min extension reaction. Therefore, target m⁶A DNA could not effectively be distinguished only depending on the impediment of m⁶A to DNA synthesis. As shown in Fig. 2B, when KF exo⁻, Ag^I, dNTPs (without dTTP), and dsDNA

were mixed at 37 °C for 10 min (lane 4 and 5), 15 min (lane 6 and 7) and 20 min (lane 8 and 9). Lane 4–7 indicated that dsDNA-1 was extended, but the extension of dsDNA-2 was hindered. Thus, target m⁶A DNA was distinguished effectively based on the double-hindered replication system.

Second, each reaction process of the sensing strategy was analyzed by measuring DPV signal, and the results were depicted in Fig. 2D. Compared to blank control that did not include target A and target m⁶A DNA (curve a), a very low DPV signal was detected responding to 1 nM



target A (curve b), which was because the Ag^{I} -mediated replication blocked LP recognition domain. However, in the presence of 1 nM target m^6A DNA, a significant DPV signal was observed (curve c). This was attributed to the binding of LP@MB@Zr-MOF to LP recognition domain, generating amplified electrochemical signal. These results clearly demonstrated that the constructed biosensor possessed outstanding ability to specifically distinguish m^6A DNA.

Optimization of the experiment variables of the biosensing strategy

To obtain the best performance of the electrochemical biosensor, three important experimental parameters were optimized. First, the double-hindered replication time was evaluated. As illustrated in Fig. 3A, the DPV signal increased with the incubation time until 15 min when the signal from target m^6A DNA to background from target A (S/B) ratio reached the pinnacle. After that, the DPV signal decreased, because the DNA polymerase nonspecifically prolonged the CP if the incubation time was too long.

Second, the concentration of MB loaded on Zr-MOF was optimized. As shown in Fig. 3B, DPV signal exhibited an upward trend with the increase of MB concentration from 0.5 to 4 μM MB. However, when the concentration of MB surpassed 2 μM , an obvious background noise was observed, resulting from the nonspecific adsorption of superfluous MB on the electrode surface. Thus, the biggest S/B ratio was obtained when the concentration of MB loaded on Zr-MOF was 2 μM .

Third, we evaluated the influence of Zr-MOF concentration on DPV signal. As depicted in Additional file 1: Fig. S2, the different concentrations of Zr-MOF from 0.5 to 4 mg/mL were selected to screen the best concentration with optimal S/B ratio. Clearly, 1 mg/mL of Zr-MOF generated the most satisfactory S/B ratio that was taken as the best condition for the subsequent experiment. Next, the reaction buffer containing various concentration of AgNO_3 from 50 to 150 μM was tested. As shown in Additional file 1: Fig. S3, the DPV signal and the S/B ratio increased gradually with the concentration of AgNO_3 and reached the highest peak at 100 μM AgNO_3 . After that, the signal declined sharply. Thus, the reaction buffer containing 100 μM AgNO_3 was selected for other experiments.

Sensitivity of the developed biosensor

Under optimal experimental conditions, the sensitivity of the biosensor was analyzed in the presence of different concentrations of target m^6A DNA ranging from 1 fM to 1 nM. The DPV signal increased with the

concentration of target m^6A DNA (Fig. 4A), and the good linear relationship between the DPV response and the logarithm of target m^6A DNA concentration ranging from 1 fM to 1 nM was obtained (Fig. 4B). According to the mathematical results, the determined linear regression equation was $i = 0.85 \lg C + 1.05$ (correlation coefficient $R^2 = 0.9976$, where i and C represents DPV signal and the concentration of target m^6A DNA, respectively). The low detection of limit (LOD) for target m^6A DNA was 0.89 fM according to the 3σ rule. The LOD was lower than most of previously reported sensing methods towards m^6A DNA [14, 19, 20, 23], benefiting from the powerful signal amplification capability of MB@Zr-MOF. Moreover, the biosensor was time-saving compared to traditional strategies, the detailed discussion was depicted in Additional file 1: Table S3.

Selectivity and stability of the biosensor

The selectivity of the proposed strategy was evaluated by replacing A site with normal T, C, and G bases, which were corresponding to target T, target C, and target G, respectively. As shown in Fig. 5A, the DPV signals of these interfering sequences were substantially identical to that of target A, and negligible change of electrochemical signal was observed. Nevertheless, the DPV signal of target m^6A DNA had a significant increase, which was about 4.5-fold higher than that of these interfering sequences. These results demonstrated that the strategy exhibited high fidelity in discriminating target m^6A DNA and other unmodified genomic DNA, which was attributed to the good selectivity of double-hindered replication towards target m^6A DNA.

Furthermore, the stability of the developed biosensor was evaluated. Owing to acidic and alkaline condition may destroy the structure of LP@MB@Zr-MOF and disturb the loading of MB, pH could be a key parameter for the stability of the biosensor. As shown in Fig. 5B, the LP@MB@Zr-MOF could maintain stabilization with pH values changing from 6 to 8, and the highest DPV signal was obtained when the pH was about 8. In addition, the peak current values almost kept unchanged though the components of the developed biosensor were stored at 4 $^{\circ}\text{C}$ for 15 days (Additional file 1: Fig. S4). These results demonstrated that the good stability of the develop biosensor.

Clinical applicability of the biosensor

To assess the applicability of the electrochemical biosensor towards detection of target m^6A DNA in physiological environment, the recovery test was firstly

carried out. In standard addition experiments, the comparable results of different concentrations of target m⁶A DNA at 10 fM, 1 pM, 100 pM in 20-fold diluted serum was illustrated in Additional file 1: Table S2. The recoveries rate was in the range of 96.65–103.02%, and the RSD was in the range of 4.34–5.87%. Furthermore, in order to test the applicability of this biosensor in real cells, the m⁶A DNA expressed in HepG2 cells and NeHepLxHT cells was analyzed by our developed method and ELISA kit [11]. As shown in Additional file 1: Fig. S5, with the increasing of concentration of HepG2 cells (a–c), the corresponding DPV signals increased proportionably, suggesting that the produced signal was highly dependent on the concentration of m⁶A DNA in HepG2 cells. And the signal of HepG2 cells (c) was obviously higher than that of NeHepLxHT cells (d) at the same concentration, which was matched with the previous reports [37]. Furthermore, the results of the electrochemical biosensor were consistent with that of ELISA kit. What's more, compared with the commercial ELISA kit whose price is about RMB 6000–7000 for 48 assays [38], the proposed biosensor is much cheaper. These results proved that the proposed biosensor exhibited reliable capacity for sensing m⁶A DNA in cells and possessed great potential in clinical application.

Conclusions

In summary, an ultrasensitive electrochemical biosensor for locus-specific detection of m⁶A DNA was developed based on double-hindered replication with nucleic acid-functioned MB@Zr-MOF. Integrating the impediment of m⁶A to DNA synthesis and the termination of m⁶A–Ag^I–C mismatch's instability to DNA replication, the biosensing strategy exhibited excellent performance in distinguishing between A site and m⁶A site. Utilizing MB@Zr-MOF as amplified signal indicator, the sensitivity of the biosensor was significantly improved, displaying LOD as low as femtomole level for analyzing m⁶A DNA. The developed method can be extended to detect m⁶A RNA in principle. Given the high sensitivity and excellent specificity, the electrochemical biosensor is a facile and alternative platform for the m⁶A DNA detection and biomedical researches. Despite these achievements, this developed strategy needs further optimization. For example, the relatively complicated synthesis of nucleic acid-functioned MB@Zr-MOF may limit its applications.

Abbreviations

m⁶A: N⁶-methyladenine; MB: Methylene blue; MOFs: Metal–organic frameworks; HCR: Hybridization chain reaction; RCA: Rolling circle amplification;

CP: Capture probes; KF exo[−]: Klenow Fragment DNA polymerase (3' → 5' exo[−]); LP: Linker probes; PBS: Phosphate buffer saline; MCH: Mercapto hexanol; HepG2: Hcuman hepatocellular carcinomas; CV: Cyclic voltammetry; EIS: Electrochemical impedance spectroscopy; DPV: Differential pulse voltammetry; PAGE: Polyacrylamide gel electrophoresis; DMEM: Dulbecco's modified eagle medium; TEM: Transmission electron microscopy; FT-IR: Fourier transform infrared spectra; LOD: Limit of detection.

Supplementary Information

The online version contains supplementary material available at <https://doi.org/10.1186/s12951-021-01156-0>.

Additional file 1: Table S1. DNA Sequences used in the experiment for established electrochemical biosensor. **Table S2.** The recoveries determined using the strategy by spiking m⁶A DNA into human serum samples. **Table S3.** The comparison of this method with other reports. **Figure S1.** Characterization of the modification procedure on an electrode. (A) CV and (B) EIS at (a) the bare GE, (b) capture probes immobilized electrode, (c) after blocked with MCH, (d) after hybridized with m⁶A DNA, (e) after hybridized with LP@MB@MOF. **Figure S2.** Optimization of the concentration of Zr-MOF. All results expressed as mean ± standard variation (n = 3). **Figure S3.** Optimization of the concentration of AgNO₃. All results expressed as mean ± standard variation (n = 3). **Figure S4.** Evaluation of the stability of the developed biosensor. All results are expressed as mean ± standard variation (n = 3). **Figure S5.** Evaluation of the applicability of the developed biosensor in real cells. DNA extraction from 1 × 10⁶ HepG2 cells with (a) 10-times dilution, (b) 5-times dilution, and (c) original value, and (d) DNA extraction from 1 × 10⁶ NeHepLxHT cells. All results are expressed as mean ± standard variation (n = 3).

Acknowledgements

This work was funded by the financial support from the National Natural Science Foundation of China (81873980), the National Science and Technology Major Project of the Ministry of Science and Technology of China (2018ZX10732202), and the Natural Science Foundation Project of Chongqing (cstc2018jcyjAX0349).

Authors' contributions

QZ, TW, XL, and HQ performed all electrochemical biosensor experimental work. QZ, HQ, XL, XB and HB conducted data analysis and manuscript revisions. TW and XL provided serum samples. SD and YY procured funding and provided project guidance. All authors read and approved the final manuscript.

Availability of data and materials

All data generated and analyzed during this study are included in this published article and additional file. The additional file is available. DNA Sequences used in the experiment for established electrochemical biosensor (Additional file 1: Table S1). The recoveries determined using the strategy by spiking m⁶A DNA into human serum samples (Additional file 1: Table S2). The comparison of this method with other reports (Additional file 1: Table S3). Characterization of the modification procedure on an electrode (Additional file 1: Figure S1). Optimization of the concentration of Zr-MOF and AgNO₃ (Additional file 1: Figures S2, S3). Evaluation of the stability of the developed biosensor (Additional file 1: Figure S4). Evaluation of the applicability of the developed biosensor (Additional file 1: Figure S5).

Declarations

Ethics approval and consent to participate

This study has been approved by the ethics committee of Chongqing Medical University and conducted in accordance with ethical guidelines.

Consent for publication

All authors agree to be published.

Competing interests

The authors declare that they have no competing interests.

Author details

¹Key Laboratory of Clinical Laboratory Diagnostics (Ministry of Education), College of Laboratory Medicine, Chongqing Medical University, Chongqing 400016, China. ²Department of Laboratory Medicine, Chongqing Hospital of Traditional Chinese Medicine, Chongqing 400016, China.

Received: 11 August 2021 Accepted: 21 November 2021

Published online: 07 December 2021

References

- Sun M, Song MM, Wei B, Gao Q, Li L, Yao B, Chen L, Lin L, Dai Q, Zhou X, et al. 5-Hydroxymethylcytosine-mediated alteration of transposon activity associated with the exposure to adverse in utero environments in human. *Hum Mol Genet.* 2016;25:2208–19.
- Skvortsova K, Iovino N, Bogdanović O. Functions and mechanisms of epigenetic inheritance in animals. *Nat Rev Mol Cell Biol.* 2018;19:774–90.
- Chen Y, Hong T, Wang S, Mo J, Tian T, Zhou X. Epigenetic modification of nucleic acids: from basic studies to medical applications. *Chem Soc Rev.* 2017;46:2844–72.
- Summerer D. N⁶-methyladenine: a potential epigenetic mark in eukaryotic genomes. *Angew Chem Int Ed.* 2015;54:10714–6.
- Smith ZD, Meissner A. DNA methylation: roles in mammalian development. *Nat Rev Genet.* 2013;14:204–20.
- Xiao CL, Zhu S, He M, Chen D, Zhang Q, Chen Y, Yu G, Liu J, Xie SQ, Luo F, et al. N(6)-methyladenine DNA modification in the human genome. *Mol Cell.* 2018;71:306–318307.
- Collier J, McAdams HH, Shapiro L. A DNA methylation ratchet governs progression through a bacterial cell cycle. *Proc Natl Acad Sci USA.* 2007;104:17111–6.
- Marinus MG, Casadesus J. Roles of DNA adenine methylation in host-pathogen interactions: mismatch repair, transcriptional regulation, and more. *FEMS Microbiol Rev.* 2009;33:488–503.
- Heithoff DM, Sinsheimer RL, Low DA, Mahan MJ. An essential role for DNA adenine methylation in bacterial virulence. *Science.* 1999;284:967–70.
- Liu T, Wei Q, Jin J, Luo Q, Liu Y, Yang Y, Cheng C, Li L, Pi J, Si Y, et al. The m6A reader YTHDF1 promotes ovarian cancer progression via augmenting EIF3C translation. *Nucleic Acids Res.* 2020;48:3816–31.
- Chen M, Wong C-M. The emerging roles of N⁶-methyladenosine (m6A) deregulation in liver carcinogenesis. *Mol Cancer.* 2020;19:44.
- Xie Q, Wu T, Gimple R, Li Z, Prager B, Wu Q, Yu Y, Wang P, Wang Y, Gorkin D, et al. N-methyladenine DNA modification in glioblastoma. *Cell.* 2018;175:1228–1243.e1220.
- Bhattacharjee R, Moriam S, Nguyen N-T, Shiddiky MJA. A bisulfite treatment and PCR-free global DNA methylation detection method using electrochemical enzymatic signal engagement. *Biosens Bioelectron.* 2019;126:102–7.
- Hong T, Yuan Y, Wang T, Ma J, Yao Q, Hua X, Xia Y, Zhou X. Selective detection of N⁶-methyladenine in DNA via metal ion-mediated replication and rolling circle amplification. *Chem Sci.* 2017;8:200–5.
- Greer Eric L, Blanco Mario A, Gu L, Sendinc E, Liu J, Aristizábal-Corrales D, Hsu C-H, Aravind L, He C, Shi Y. DNA methylation on N⁶-adenine in *C. elegans*. *Cell.* 2015;161:868–78.
- Fang G, Munera D, Friedman DI, Mandlik A, Chao MC, Banerjee O, Feng Z, Losic B, Mahajan MC, Jabado OJ, et al. Genome-wide mapping of methylated adenine residues in pathogenic *Escherichia coli* using single-molecule real-time sequencing. *Nat Biotechnol.* 2012;30:1232–9.
- Luo G-Z, Wang F, Weng X, Chen K, Hao Z, Yu M, Deng X, Liu J, He C. Characterization of eukaryotic DNA N(6)-methyladenine by a highly sensitive restriction enzyme-assisted sequencing. *Nat Commun.* 2016;7:11301.
- Boulias K, Greer E. Detection of DNA methylation in genomic DNA by UHPLC-MS/MS. *Methods Mol Biol.* 2021;2198:79–90.
- Chen Y-A, Oblisca JM, Liu Y-L, Liu C, Gwozdz ML, Yeh H-C. NanoCluster beacons enable detection of a single N⁶-methyladenine. *J Am Chem Soc.* 2015;137:10476–9.
- Wang S, Wang J, Zhang X, Fu B, Song Y, Ma P, Gu K, Zhou X, Zhang X, Tian T, Zhou X. Methyladenine hinders RNA- and DNA-directed DNA synthesis: application in human rRNA methylation analysis of clinical specimens. *Chem Sci.* 2016;7:1440–6.
- Funai T, Miyazaki Y, Aotani M, Yamaguchi E, Nakagawa O, Wada S, Torigoe H, Ono A, Urata H. Ag(I) ion mediated formation of a C-A mispair by DNA polymerases. *Angew Chem.* 2012;51:6464–6.
- Santamaría-Díaz N, Méndez-Arriaga JM, Salas JM, Galindo MA. Highly stable double-stranded DNA containing sequential Silver(I)-mediated 7-Deazaadenine/Thymine Watson-Crick Base Pairs. *Angew Chem.* 2016;55:6170–4.
- Wang Y, Zheng J, Duan C, Jiao J, Gong Y, Shi H, Xiang Y. N detection of locus-specific-methyladenosine modification based on Ag-assisted ligation and supersandwich signal amplification. *Analyst.* 2021;146:1355–60.
- Deng R, Tang L, Tian Q, Wang Y, Lin L, Li J. Toehold-initiated rolling circle amplification for visualizing individual microRNAs in situ in single cells. *Angew Chem.* 2014;53:2389–93.
- Lv Y, Cui L, Peng R, Zhao Z, Qiu L, Chen H, Jin C, Zhang X, Tan W. Entropy beacon: a hairpin-free DNA amplification strategy for efficient detection of nucleic acids. *Anal Chem.* 2015;87:11714–20.
- Morris W, Briley W, Auyeung E, Cabezas M, Mirkin C. Nucleic acid-metal organic framework (MOF) nanoparticle conjugates. *J Am Chem Soc.* 2014;136:7261–4.
- Wang S, McGuirk C, Ross M, Wang S, Chen P, Xing H, Liu Y, Mirkin C. General and direct method for preparing oligonucleotide-functionalized metal-organic framework nanoparticles. *J Am Chem Soc.* 2017;139:9827–30.
- Tian T, Zeng Z, Vulpe D, Casco M, Divitini G, Midgley P, Silvestre-Alberio J, Tan J, Moghadam P, Fairen-Jimenez D. A sol-gel monolithic metal-organic framework with enhanced methane uptake. *Nat Mater.* 2018;17:174–9.
- Mallick A, El-Zohry A, Shekha O, Yin J, Jia J, Aggarwal H, Emwas A, Mohammed O, Eddaoudi M. Unprecedented ultralow detection limit of amines using a thiazole-functionalized Zr(IV)-based metal-organic framework. *J Am Chem Soc.* 2019;141:7245–9.
- Bai Y, Dou Y, Xie L, Rutledge W, Li J, Zhou H. Zr-based metal-organic frameworks: design, synthesis, structure, and applications. *Chem Soc Rev.* 2016;45:2327–67.
- Yan D, Lou Y, Yang Y, Chen Z, Cai Y, Guo Z, Zhan H, Chen B. Dye-modified metal-organic framework as a recyclable luminescent sensor for nicotine determination in urine solution and living cell. *ACS Appl Mater Interfaces.* 2019;11:47253–8.
- Chang J, Wang X, Wang J, Li H, Li F. Nucleic acid-functionalized metal-organic framework-based homogeneous electrochemical biosensor for simultaneous detection of multiple tumor biomarkers. *Anal Chem.* 2019;91:3604–10.
- Yan B. Lanthanide-functionalized metal-organic framework hybrid systems to create multiple luminescent centers for chemical sensing. *Acc Chem Res.* 2017;50:2789–98.
- Chen W, Yu X, Cecconello A, Sohn Y, Nechushtai R, Willner I. Stimuli-responsive nucleic acid-functionalized metal-organic framework nanoparticles using pH- and metal-ion-dependent DNAzymes as locks. *Chem Sci.* 2017;8:5769–80.
- Wang Y, Yin H, Li X, Waterhouse GIN, Ai S. Photoelectrochemical immunosensor for N(6)-methyladenine detection based on Ru@UiO-66, Bi₂O₃ and Black TiO₂. *Biosens Bioelectron.* 2019;131:163–70.
- Gao D, Chen J-H, Fang S, Ma T, Qiu X-H, Ma J-G, Gu Q, Cheng P. Simultaneous quantitative recognition of all purines including N⁶-methyladenine via the host-guest interactions on a Mn-MOF. *Matter.* 2021;4:1001–16.
- Zhang C, Huang S, Zhuang H, Ruan S, Zhou Z, Huang K, Ji F, Ma Z, Hou B, He X. YTHDF2 promotes the liver cancer stem cell phenotype and cancer metastasis by regulating OCT4 expression via m6A RNA methylation. *Oncogene.* 2020;39:4507–18.
- Ouyang L, Su X, Li W, Tang L, Zhang M, Zhu Y, Xie C, Zhang P, Chen J, Huang H. ALKBH1-demethylated DNA N6-methyladenine modification triggers vascular calcification via osteogenic reprogramming in chronic kidney disease. *J Clin Invest.* 2021;131:e146985.

Publisher's Note

Springer Nature remains neutral with regard to jurisdictional claims in published maps and institutional affiliations.